ORIGINAL ARTICLE

Claudin targeting as an effective tool for directed barrier modulation of the viable epidermis

Laura-Sophie Beier[1,2] | **Ayk Waldow**[1] | **Saeed Khomeijani Farahani**[1] |
Roman Mannweiler[1] | **Sabine Vidal-Y-Sy**[3] | **Johanna M. Brandner**[3] | **Jörg Piontek**[1] |
Dorothee Günzel[1]

[1]Clinical Physiology/Nutritional Medicine, Medical Department, Division of Gastroenterology, Infectiology, Rheumatology, Charité - Universitätsmedizin Berlin, Berlin, Germany

[2]Laboratory of Mucosal Barrier Pathobiology, Department of Pathology, Brigham and Women's Hospital and Harvard Medical School, Boston, Massachusetts, USA

[3]Department of Dermatology and Venerology, University Hospital Hamburg-Eppendorf, Hamburg, Germany

Correspondence
Dorothee Günzel and Jörg Piontek, Clinical Physiology/Nutritional Medicine, Medizinische Klinik für Gastroenterologie, Infektiologie und Rheumatologie, Charité – Universitätsmedizin, Campus Benjamin Franklin, Hindenburgdamm 30, 12203 Berlin, Germany.
Email: dorothee.guenzel@charite.de and joerg.piontek@charite.de

Laura-Sophie Beier and Ayk Waldow share first authorship.

Jörg Piontek and Dorothee Günzel share last authorship.

Abstract

Tight junction (TJ) formation is vital for epidermal barrier function. We aimed to specifically manipulate TJ barriers in the reconstructed human epidermis (RHE) by claudin-1 and -4 knockdown (KD) and by claudin-binding fusion proteins of glutathione *S*-transferase and modified C-terminal fragments of *Clostridium perfringens* enterotoxin (GST-cCPE). Impedance spectroscopy and tracer permeability imaging were employed for functional barrier assessment and investigation of claudin contribution. KD of claudin-1, but not claudin-4, impaired the paracellular barrier *in vitro*. Similarly, claudin-binding GST-cCPE variants weakened the paracellular but not the stratum corneum barrier. Combining both TJ targeting methods, we found that claudin-1 targeting by GST-cCPE after claudin-4 KD led to a marked decrease in paracellular barrier properties. Conversely, after claudin-1 KD, GST-cCPE did not further impair the barrier. Comparison of GST-cCPE variants with different claudin-1/claudin-4 affinities, NHS-fluorescein tracer detection, and immunostaining of RHE paraffin sections showed that GST-cCPE variants bind to extrajunctional claudin-1 and -4, which are differentially distributed along the stratum basale–stratum granulosum axis. GST-cCPE binding blocks these claudins, thereby specifically opening the paracellular barrier of RHE. The data indicate a critical role for claudin-1 in regulating paracellular permeability for ions and small molecules in the viable epidermis. Claudin targeting is presented as a proof-of-concept for precise barrier modulation.

KEYWORDS
claudin targeting, epidermal barrier, epidermis, impedance spectroscopy, tight junctions

INTRODUCTION

The epidermis provides a tight barrier separating the body from the external environment. It plays a crucial role in protecting the body against external influences, such as pathogens, xenobiotics, and UV radiation, while at the same time preventing dehydration due to uncontrolled transepidermal water loss.[1,2] The epidermis is a stratified epithelium, which undergoes a constant and dynamic turnover
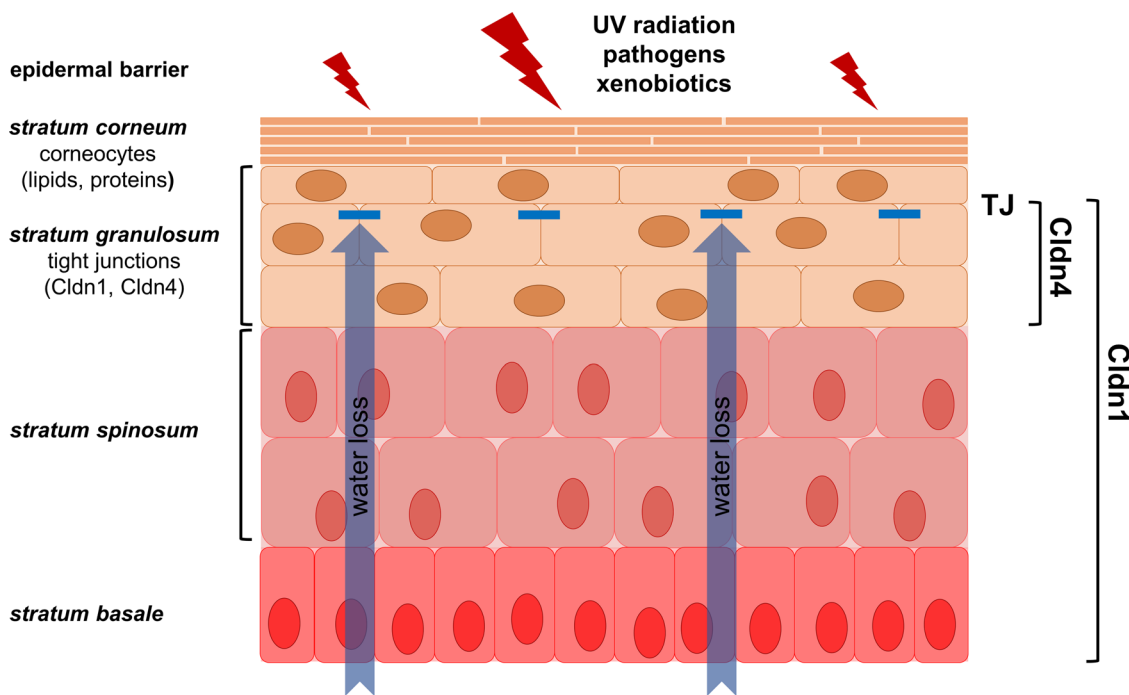
FIGURE 1 The epidermal barrier. The epidermis is a stratified epithelium preventing harmful substances from entering the body and extensive water loss to occur via the skin. The epidermal barrier is formed by a tight seal of corneocytes, proteins, and lipids in the *stratum corneum* (SC barrier), and the TJs, sealing the paracellular space between viable cells in the second layer of the *stratum granulosum*.[1,33]

to maintain its barrier function. This turnover is driven by proliferating keratinocytes in the basal layer. Upon induction of differentiation, the keratinocytes move upward through the spinal (stratum spinosum) and granular (stratum granulosum, SG) layer while undergoing a terminal differentiation process that ultimately leads to the formation of the stratum corneum (SC), a tight layer of dead, cornified keratinocytes (corneocytes), lipids, and proteins that is in direct contact with the external environment and provides crucial structural and innate immune barrier properties (Figure 1).[1,3]

Whereas the SC had long been identified as a major structural barrier component, the contribution of structural barrier elements in the viable epidermis (VE) to the epidermal barrier has only been recognized during the past two decades. It is now appreciated that the tight junctions (TJs) between viable cells in the granular layer form an essential barrier that is crucial to ensure proper barrier function, especially with respect to transepidermal water loss.[4,5] TJs are well characterized in simple epithelia, such as the intestinal epithelium or the kidney tubules, where they form a size- and charge-selective paracellular barrier preventing uncontrolled diffusion of water and solutes. Conventionally, claudins have been categorized as either channel- or barrier-forming. Hence, depending on the claudin composition, a specific epithelium might be rather tight or leaky.[6] In the human epidermis, claudin-1 (Cldn1) and claudin-4 (Cldn4) are the main TJ-constituting claudins.[4,7,8] Cldn1 has consistently been classified as a barrier-forming claudin,[4] reflecting the tightly sealed nature of the epidermis. The function of Cldn4 is still under debate.[9] However, it is mostly regarded to be barrier forming.[9,10]

The importance of the two epidermal barriers is underlined in numerous skin diseases associated with an explicit barrier dysfunction. Disease-related alterations of the SC components (e.g., filaggrin and ceramides) have been well described in atopic and contact dermatitis,[11–13] ichthyosis,[14] and psoriasis.[15] Importantly, many of these diseases are also characterized by downregulation in the expression of TJ protein Cldn1 and altered expression of Cldn4 in the VE.[7,16–18] Furthermore, the neonatal ichthyosis-sclerosing cholangitis syndrome, an autosomal-recessive disease with epidermal and liver-associated symptoms, is caused by mutations in human Cldn1.[19] The relevance of the epidermal TJ barrier is further emphasized considering that Cldn1-deficient mice die within 1 day after birth due to tremendous transepidermal water loss and dehydration.[4] Notwithstanding, a directed and reversible opening of the epidermal barrier could be useful to enhance transdermal drug delivery,[20] in a similar way as it has been described for enhanced drug delivery across the blood–brain barrier.[21,22] Therefore, dissecting and understanding the contributions of the individual components to the overall epidermal barrier is critical to the success of efforts to treat barrier-linked skin diseases and modulate epidermal permeability in a targeted manner.

However, a detailed understanding of the contribution and, possibly, cooperation of individual barrier components in the epidermis is still lacking. Conventional methods to characterize the overall skin barrier include transepidermal water loss,[23] transepithelial electrical resistance,[24,25] dye penetration assays,[3] and permeation of locally applied drugs.[26,27] A major drawback of these techniques is their

inability to differentiate between the barrier properties of the SC and VE, including the TJs.

Variants of the C-terminal, claudin-binding domain of *Clostridium perfringens* enterotoxin (cCPE) are molecular tools to specifically modulate the TJ barrier of epithelia in a claudin-dependent and subtype-specific manner[28] (Figure S1). Modifications of cCPE enabled targeting of a wide range of claudins. Whereas the wild-type binds with high affinity to Cldn3 and -4 but not or only weakly to other claudins, such as Cldn1,[29,30] the triple mutant cCPE-S305P/S307R/S313H (cCPE-SSS) has a high affinity for a broad spectrum of claudins (Cldn1–9).[31,32] cCPE variants have been shown to modulate TJs in physiologically relevant barriers, like the blood–brain barrier[21,22] or the epidermal barrier.[24] Standard transepithelial resistance (TER) measurement revealed that claudin-binding cCPE variants impaired the ion barrier at early and later stages of epidermal differentiation, whereas permeability for Lucifer Yellow was only affected at early stages of stratification and responded stronger when both Cldn1 and -4 were targeted (cCPE-SSS).[24] So far, the effect of cCPE variants on the epidermal barrier could not be attributed directly to TJ-modulating effects as such measurements were not possible.

In the present study, we applied a noninvasive impedance spectroscopy method that allows the separate resolution of the SC and VE barrier,[33] and combined it with directed modulation of the TJ barrier in the VE via siRNA-mediated knockdown (KD) of Cldn1 and -4 as well as claudin blocking by cCPE variants. We used models of the reconstructed human epidermis (RHE) as an easily adjustable *in vitro* model, which displays a stratified morphology comparable to the native epidermis and enabled the identification of barrier components.[7,33,34] Our results clearly support the contribution of the TJs to the overall epidermal barrier and suggest distinct roles for Cldn1 and -4 in the epidermis. Claudin targeting by cCPE variants enabled moderate and specific modulation of the VE barrier without affecting SC and overall tissue integrity.

MATERIALS AND METHODS

Reconstructed human epidermis

Primary keratinocytes for the generation of RHE were obtained anonymously during surgical removal of juvenile foreskin from young male donors (younger than 5 years) with written and informed consent from their legal guardians. Approval from the ethics committee of the Ärztekammer Hamburg was granted (WF-61/12). All investigations were conducted in accordance with the principles expressed in the Declaration of Helsinki.

RHE were cultivated as described before.[34] Primary keratinocytes were isolated from juvenile foreskin and expanded in submerged culture for three passages. To generate RHE, 2×10^5 keratinocytes were seeded onto cell culture inserts (0.6 cm^2 area, 400 nm pore size, Merck Millipore) in 500 µl of EpiLife Medium (supplemented with 1.5 mM CaCl$_2$, Life Technologies) and placed in 6-well plates. The basal compartment was filled with 2.5 ml EpiLife medium with 1.5 mM CaCl$_2$.

After 30 h of cultivation at 37°C in a humidified atmosphere, cells were lifted to an air–liquid interface (ALI) and the medium in the basal compartment was changed to EpiLife medium containing 1.5 mM CaCl$_2$, 92 µg/ml ascorbic acid (Merck), and 10 ng/ml recombinant human keratinocyte growth factor (R&D Systems). The medium was changed every other day and experiments were performed at day 4 after lifting to ALI.

siRNA-mediated KD of claudin-1 and -4

Confluent primary keratinocytes in passage 3 were trypsinized, resuspended in EpiLife medium containing 1.5 mM CaCl$_2$, and transfected in suspension by using HiPerFect transfection reagent (Qiagen) and siRNAs for human Cldn1 (Hs_CLDN1_8: SI04279114), human Cldn4 (Hs_CLDN4_7: SI03064418), or AllStars negative control (siRNA ctrl; SI03650318). siRNAs were purchased from Qiagen; their effectiveness had been shown previously.[7,35] Transfected cells were directly used to build RHE.

Lysis and western blot of RHE models

Protein expression levels in RHE models were determined by immunoblotting. On day 5 after lifting to ALI, the stratified cell layers were lysed in RIPA buffer (50 mM Tris, 150 mM NaCl, 5 mM EDTA, 0.5% [w/v] sodium deoxycholate, 0.1% [w/v] SDS, 1% [v/v] Nonidet P-40, and cOmplete™ EDTA-free protease inhibitor cocktail; Roche, Germany, adjusted to pH 7.5), scraped off filters, and transferred into tubes. After centrifugation ($14,000 \times g$, 15 min, 4°C), the supernatant was collected and protein concentrations were determined via Pierce™ BCA Assay Kit (Thermo Fisher Scientific, Waltham, MA, USA). Per lysate 20 µg of proteins were heated in Laemmli buffer at 95°C for 5 min and loaded onto 12.5% SDS-PAGE gels. After separation via gel electrophoresis, samples were transferred onto PVDF membranes. Proteins were probed via rabbit anti-Cldn1 (1:1000, #51-9000, Invitrogen, Thermo Fisher), rabbit anti-Cldn4 (1:1000, #36-4800, Thermo Fisher Inc.), and mouse anti-b-Actin (1:10,000, #A5441, Merck, Germany). Primary antibodies were detected via goat anti-rabbit HRP-conjugated F(ab')2 fragment (1:10,000, #111-036-003, Jackson ImmunoResearch, UK) and goat anti-mouse HRP-conjugated F(ab')2 Fragment (1:10,000, #115-036-003, Jackson ImmunoResearch). Blot detection by chemiluminescence was performed with SuperSignal West Pico PLUS substrate (Thermo Fisher Scientific) in a Fusion FX (Vilber, Germany). Densitometric analysis was performed using ImageJ 1.53q.

Expression and purification of GST-cCPE fusion proteins

Claudin targeting was achieved by fusion proteins of glutathione *S*-transferase (GST) and different cCPE variants. This enabled fast

and efficient purification via a glutathione agarose column, while also increasing the solubility of cCPE (unpublished initial studies). GST-cCPE variants with known affinities for different claudins[24,32,36] have been successfully used for targeted modulation of the paracellular barrier in different *in vitro* models.[21,24,37] Plasmids encoding GST-cCPEwt[194−319] (GST-cCPE), GST-cCPE-S305P/S307R/S313H (GST-cCPE-SSS), and GST-cCPE-Y306A/L315A (GST-cCPE-YL) were reported previously.[32] GST-cCPE fusion proteins from these plasmids were expressed in *E. coli* BL21 and purified as described.[32] In short, bacteria were grown to an optical density of 0.6−0.8, when the expression was induced by the addition of 1 mM isopropyl-β-D-thiogalactopyranoside. Three hours after induction, bacteria were harvested, lysed in lysis buffer (phosphate-buffered saline [PBS] with 1% [v/v] Triton X-100, 0.1 mM phenylmethylsulfonyl fluoride, 1 mM ethylenediaminetetraacetic acid, protease inhibitor cocktail [cOmplete™, Mini Protease Inhibitor Cocktail, final concentration 1 ×, Merck]), and sonicated by 15 × 1 s pulses (Vibra Cell. Model 72434 BioBlock Scientific). Insoluble cell debris was removed by centrifugation (20,000 × *g*, 30 min, 4°C) and GST-proteins were purified from the supernatant using glutathione agarose (Sigma-Aldrich) and dialyzed against PBS. Protein concentration was determined using the Pierce™ BCA Assay Kit (Thermo Fisher Scientific).

Cellular GST-cCPE-binding assay to determine equilibrium dissociation constants

Native HEK293 cells lack endogenous claudins, rendering them a suitable model to test claudin targeting and affinity of cCPE variants. Cellular GST-cCPE-binding assays were performed and equilibrium dissociation constants (K_D) were determined as previously described.[32,38] HEK293 cell clones stably transfected with p3xFlag-CMV-10/huCldn4 were used after Cldn4 expression was verified via immunofluorescence staining and western blot. The cells were incubated with different concentrations of GST-cCPE constructs (0−1000 nM, 37°C, 30 min) in 24-well plates. Cells were fixed (4% [w/v] paraformaldehyde, 10 min), followed by washing and quenching. Bound GST-cCPE was detected via PhycoLink® anti-GST-R-phycoerythrin conjugate and normalized to cell number (Hoechst 33342). Normalized fluorescence intensity of bound anti-GST antibody was plotted against GST-cCPE concentration. The K_D was calculated using nonlinear regression analysis for a single-site, specific binding in GraphPad Prism version 7.0 (San Diego, CA, USA). Unspecific binding was accounted for by subtracting the fluorescence signal after incubation of untransfected HEK293 cells with respective concentrations of GST-cCPE. We then applied Welch's *t*-test to determine significant differences between K_D values of GST-cCPE-SSS and GST-cCPEwt. Although we cannot exclude that the GST tag might have an influence on cCPE binding to its receptor claudins, previously determined K_D values for GST-cCPE are in the same range as for His-tagged cCPE and full-length CPE.[24,30,32,39−41] Exclusively using GST-cCPE variants in this study serves as an internal control and standard.

Treatment of RHE with GST-cCPE variants and barrier assays

Four days after transitioning to ALI, 1, 10, or 50 μg/ml of the GST-cCPE variants (GST-cCPEwt, GST-cCPE-S305P/S307R/S313H [GST-cCPE-SSS], or GST-cCPE-Y306A/L315A [GST-cCPE-YL]) were added to the basal compartment of the RHE models. After 24 h of incubation at 37°C in a humidified atmosphere, impedance spectra were recorded using agarose-embedded electrolyte.[33]

Following impedance measurements, the basal medium was exchanged to 0.5 mg/ml NHS-fluorescein paracellular tracer molecule in PBS and incubated for 40 min, followed by fixation in 4% PFA.

Immunofluorescence staining

Dehydration and paraffin embedding of fixed RHE were performed by the iPATH.Berlin Core Facility. Paraffin sections were prepared at 3 μm thickness on a Leica SM2010R sliding microtome. After deparaffinization and antigen retrieval, immunofluorescence staining was performed for Cldn4 (rabbit anti-Cldn-4 #36-4800 and mouse anti Cldn4 #32-9400, Invitrogen, Thermo Fisher Scientific), Cldn1 (rabbit anti-Cldn-1 #51-9000, Invitrogen, Thermo Fisher Scientific), occludin (rabbit anti-occludin #71-1500, Invitrogen, Thermo Fisher Scientific), zonula occludens (ZO1) (mouse anti-ZO1 #33-9100, Invitrogen, Thermo Fisher Scientific) and GST-cCPE via the GST-tag (mouse anti-GST, SAB5300159, Sigma-Aldrich, Saint Louis, MO, USA). Alexa Fluor™ 488 goat anti-rabbit, Alexa Fluor™ 594 goat anti-mouse, and Alexa Fluor™ 647 goat anti-rabbit were used as secondary antibodies (Invitrogen, Thermo Fisher Scientific).

Image acquisition and analysis

Image acquisition was performed with a Zeiss Plan-Apochromat 20×/0.8 NA objective on a Zeiss LSM780. To assess the permeability of the NHS-fluorescein tracer molecule through the TJ, the apical and basal membrane-associated fluorescence intensity of the second cell layer of stratum granulosum (SG2) was measured. TJs were determined by Cldn4 staining patterns in conjunction with the NHS-fluorescein signal. In ZEN black edition (Zeiss), each membrane signal was quantified by averaging it from three individual, manually drawn profiles. Unspecific background signals in profiles were corrected by subtracting the median of the intracellular signals.

We performed colocalization studies using ImageJ version 1.53f, and Pearson values *R* were determined via the Coloc2 plugin. For colocalization analysis, a mask from the NHS-fluorescein signal was created to limit the colocalization analysis to membrane-associated signals, excluding unspecific intracellular signals. Mask creation was achieved by first applying the subtract background algorithm for the fluorescein/488 nm excitation channel, then membrane-like structures were selected via the tubeness plugin. After binary thresholding, the

|

analyze particle plugin was applied, adjusting it to select nonspherical big structures, to sort out small fragments. For each image, an individual mask was generated automatically following the above-described procedure, while the analyzed channels for GST-cCPE and Cldn1 or -4 (594 and 647 nm excitation, respectively) remained unchanged.

Impedance spectroscopy

Impedance spectroscopy was carried out essentially as previously described.[33] In brief, agar-embedded electrodes were used to apply AC currents of different frequencies (48 frequencies [f] between 1.3 Hz and 65 kHz). The shape of the resulting Nyquist plots suggested the presence of at least two time constants (τ), indicating the presence of two RC elements (parallel resistor R and capacitor C, $\tau = R \cdot C$), one describing the electrical properties of the VE, the other of the SC. The relaxation frequency at which the imaginary part of the complex impedance reaches a minimum is f_i, which equals $1/(\tau \cdot 2 \cdot \pi)$.

To determine R for each RC element, plots of the imaginary part of the impedance Z (Z_{im}) against log(f) were fitted with the following equation:

$$Z_{im} = \text{imaginary part } (R_{VE}/(1 + R_{VE} \cdot Q_{VE} \cdot \omega^n \cdot i^n))$$

$$+\text{imaginary part } (R_{SC}/(1 + R_{SC} \cdot Q_{SC} \cdot \omega^n \cdot i^n)),$$

where R_{VE} and R_{SC} are the resistance of the VE and SC, respectively; $1/[Q_{VE} \cdot (I \cdot \omega)^n]$ and $1/[Q_{SC} \cdot (i \cdot \omega)^n]$ are the impedance of a constant phase element describing the capacitive properties of the VE and SC, respectively; ω is the angular frequency ($2 \cdot \pi \cdot f$); i is $\sqrt{(-1)}$; and n is a number between 0 and 1 ($1/[Q_{SC} \cdot (i\omega)^n]$ describes a perfect capacitor for $n = 1$ and an ohmic resistor for $n = 0$).

As previously demonstrated,[33] peaks at the lower relaxation frequency f_i reflect the properties of the VE, while those at the higher relaxation frequency reflect the SC.

As capacitances reflect the properties of the lipid phase of the plasma membrane, which are unaffected by GST-cCPE treatment, alterations in R can also be expressed as shifts in log(f). As described by Mannweiler and colleagues,[33] comparing shifts in log(f) is a more robust measure if different batches of cell layers show large variations in total resistance.

Statistical analysis

Statistical analysis was performed in GraphPad Prism 7.0. For the permeability of paracellular tracer assays and colocalization studies, we tested for normal distribution by the D'Agostino–Pearson normality test. Whenever a single dataset failed the normality test, we applied the unpaired nonparametric Mann–Whitney test to the whole data set to determine statistical significance, followed by the Holm–Sidak test for multiple comparison.

Relaxation frequencies f_i from impedance measurements were analyzed by unpaired one-way ANOVA, and multiple comparison was accounted for by the Tukey test. Since relative resistances were derived from impedance measurements via peak fitting across multiple experiments, we were able to employ the paired nonparametric Wilcoxon rank sum test. Multiple comparison was accounted for by the Holm–Sidak test. All significance thresholds are set as described in the figure legends.

RESULTS

TJs are located in the SG layer in RHE

To validate our experimental system, the localization of TJ proteins was analyzed in RHE on day 5 after transitioning to ALI (Figure 2). Immunofluorescence staining confirmed the presence of Cldn1 and -4 as key claudins in the RHE, similar to human epidermis.[42,43] Cldn1 showed a strong signal in all suprabasal viable layers of RHE, which has been described previously in skin.[42,43] In contrast, Cldn4 was restricted to nucleated cells in the upper layers corresponding to the SG. Both claudins were localized over the entire plasma membrane of the keratinocytes, indicating mainly extrajunctional claudins. Nonetheless, colocalization of Cldn1 and -4 in the basolateral membrane and the absence of this colocalization in the apical membrane of keratinocytes in the SG2 layer strongly hint at intact TJs (Figure 2A, arrows).

Occludin was used as a marker for TJs in RHE. Punctate signals were found at the apex of the lateral membrane of the keratinocytes atop the Cldn4 signal as an indicator of TJ localization (Figure 2B, arrows), again similar to human skin.[42,43] In addition, a nuclear signal was detected. ZO1 is a cytoplasmic, TJ-associated protein that acts as a scaffold linking claudins to the actin cytoskeleton. Punctate, apico-lateral colocalization of ZO1 and Cldn4 (Figure 2C, arrows) is another strong indicator for functional TJs in between viable cells in the SG of RHE, similar to skin.[43]

Even though expression and localization of Cldn1 and -4 in RHE—similar to skin—is not limited to TJ structures, co-staining with the TJ-associated proteins occludin and ZO1 confirms the presence of all TJ proteins in the SG2 in RHE and strongly indicates intact TJs.

GST-cCPE variants attenuate the barrier of the VE by TJ modulation

Extrajunctional Cldn1 and -4 in the plasma membrane of keratinocytes can serve as receptors for GST-cCPE variants.[24,30,36,44] Thus, claudin capture by GST-cCPE variants enables a TJ-directed modulation of the epidermal barrier (Figure S1). Similar to a previous study,[24] we basally applied GST-cCPE variants and additionally employed impedance spectroscopy[33] to assess their effects on epidermal barrier components (Figure 3). Impedance measurement over a range of frequencies gives rise to a curve with two distinct relaxation frequency peaks.
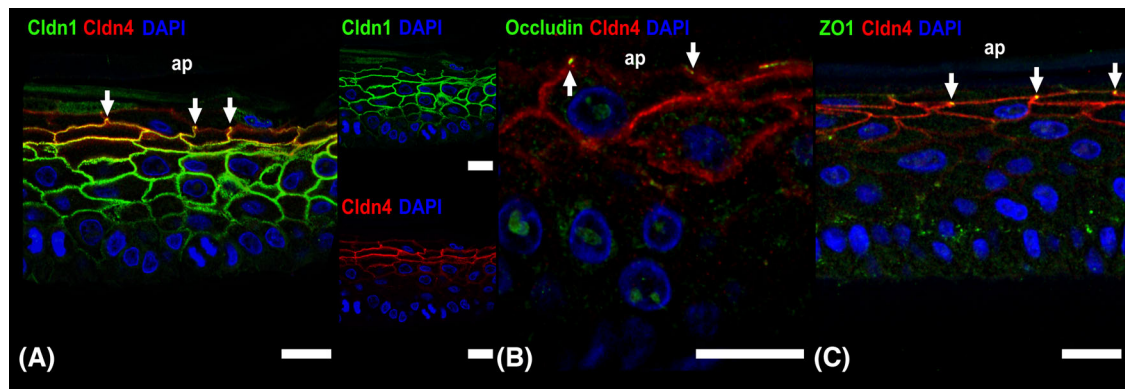
FIGURE 2 Claudin-1, - 4, occludin, and ZO1 form tight junctions in reconstructed human epidermis. Confocal microscopy images of RHE paraffin sections on day 5 after a change to ALI. (A) Cldn1 (rabbit anti-Cldn1) is expressed in all viable RHE layers, while Cldn4 (mouse anti-Cldn4) is expressed only in the upper layers (representing the stratum granulosum). A strong colocalization of Cldn1 and -4 (yellow in merged image) in the basolateral membrane together with the absence of a Cldn1 signal in the apical membrane could be an indicator of intact TJs in the SG (arrows). (B,C) The TJ markers occludin (rabbit anti-occludin) and ZO1 (mouse anti-ZO1) are localized to the apical part of the lateral membrane, to the cytoplasm, and to the nuclei of the viable keratinocytes. Localization at the apex of the lateral membrane of the keratinocytes atop the Cldn4 signal is an indicator of intact TJs (arrows). ap, apical side of the RHE facing ALI. Scale bar = 20 μm.

These correspond to the barrier of the VE and SC. Shifting of a peak to a higher frequency indicates attenuation of this epidermal barrier component.[33] Relative resistances of RHE barriers (SC and VE) after GST-cCPE treatments were derived from peak fitting (Figure 3A). Untreated RHE and treatment with 1 μg/ml GST-cCPE-Y306A/Y315A (GST-cCPE-YL, claudin binding-deficient negative control) were used as references to calculate relative resistances. Low (1 μg/ml) concentrations of claudin-binding GST-cCPE variants (-wt and -SSS) did not affect the VE barrier, whereas high (50 μg/ml) concentrations decreased the relative resistance of the VE by ∼ 50% for GST-cCPE-SSS and at least by ∼30% for GST-cCPEwt (which was not a statistically significant difference). The SC barrier was unchanged after GST-cCPE incubation, supporting a claudin-mediated effect in VE barrier modulation.

For a more robust comparison between RHE batches from different donors, we reverted to analyzing $\log_{10}(f_i)$ (as previously described by Mannweiler *et al.*;[33] Figure 3B–E) and found that in native RHE, both claudin-binding GST-cCPE variants (GST-cCPEwt and -SSS) increased $\log_{10}(f_i)$ and thus weakened the VE barrier, whereas the binding-deficient variant GST-cCPE-YL did not have any effect (Figure 3B). Analyzing $\log_{10}(f_i)$ also confirmed that incubation with GST-cCPE variants did not affect the SC barrier in any of the models (Figure 3B–E).

Further analysis aimed at discriminating between the effects of the GST-cCPE variants on a particular claudin. To this end, KD models of either Cldn1 or -4 (Figure S3; see Ref. 33) in addition to native RHE were employed. Treatment of RHE with AllStars negative control siRNA weakened both barrier components to a certain extent, which might mask any cCPE-induced effects (Figure 3C,F). Cldn1 KD prevented the formation of a tight VE barrier (Figure 3F) so that GST-cCPE-binding to the remaining claudins did not have an additional effect (Figure 3D).

Yet, when Cldn4 was knocked down, the barrier of the VE was not impaired (Figure 3F). In these models, where mostly Cldn1 was present, GST-cCPE-SSS had a slightly stronger effect on the VE barrier than GST-cCPEwt, while in native RHE, GST-cCPEwt showed a stronger effect than GST-cCPE-SSS (Figure 3B,E). This difference in effect (which did not reach statistical significance) appears to be due to the reduced expression of Cldn4 as the main receptor for cCPEwt in Cldn4 KD, hence indicating a potential role in trans-epidermal barrier maintenance for Cldn4.

Comparison of GST-cCPE–untreated RHE showed that Cldn1 KD had a pronounced effect on the epidermal barrier, whereas the barrier in Cldn4 KD models was comparable to untreated and negative control siRNA (AllStars)-treated RHE (Figure 3F).

To assess whether the barrier-weakening effects of claudin-binding GST-cCPE variants were indeed due to their binding to the extra-junctional claudins, immunofluorescence stainings of the RHE were performed, either after impedance spectroscopy (24 h) or after 48 h of incubation with GST-cCPE (Figure 4). Incubation for 24 h was sufficient for claudin-binding GST-cCPE variants to penetrate the paracellular space in all viable layers of the RHE and bind to extrajunctional Cldn1 (Figure 4A,B). Occludin was used as an indicator of TJs in the SG2. Occludin-positive spots at the apex of the basolateral membrane, where the signal of GST-cCPE (∼40 kDa) stops, represent functional TJs to larger molecules (Figure 4D,E; arrows). As GST-cCPE-YL cannot bind to claudins, there is no enriched signal at the cell–cell contacts, even though some unspecific diffusion into RHE might occur (Figure 4C,F). Co-stainings of Cldn1 or -4 and ZO1 further support the presence of TJs in the SG after treatment with claudin-binding GST-cCPE variants, suggesting that moderate claudin targeting does not destroy overall tissue integrity (Figure S2A–H).

Similar to the early time point, binding of GST-cCPEwt and -SSS was detected in all viable layers of the RHE after 48 h of incubation (Figure 4G–K). Weak and diffuse signals were also detected for GST-cCPE-YL, which can be attributed to penetration and unspecific
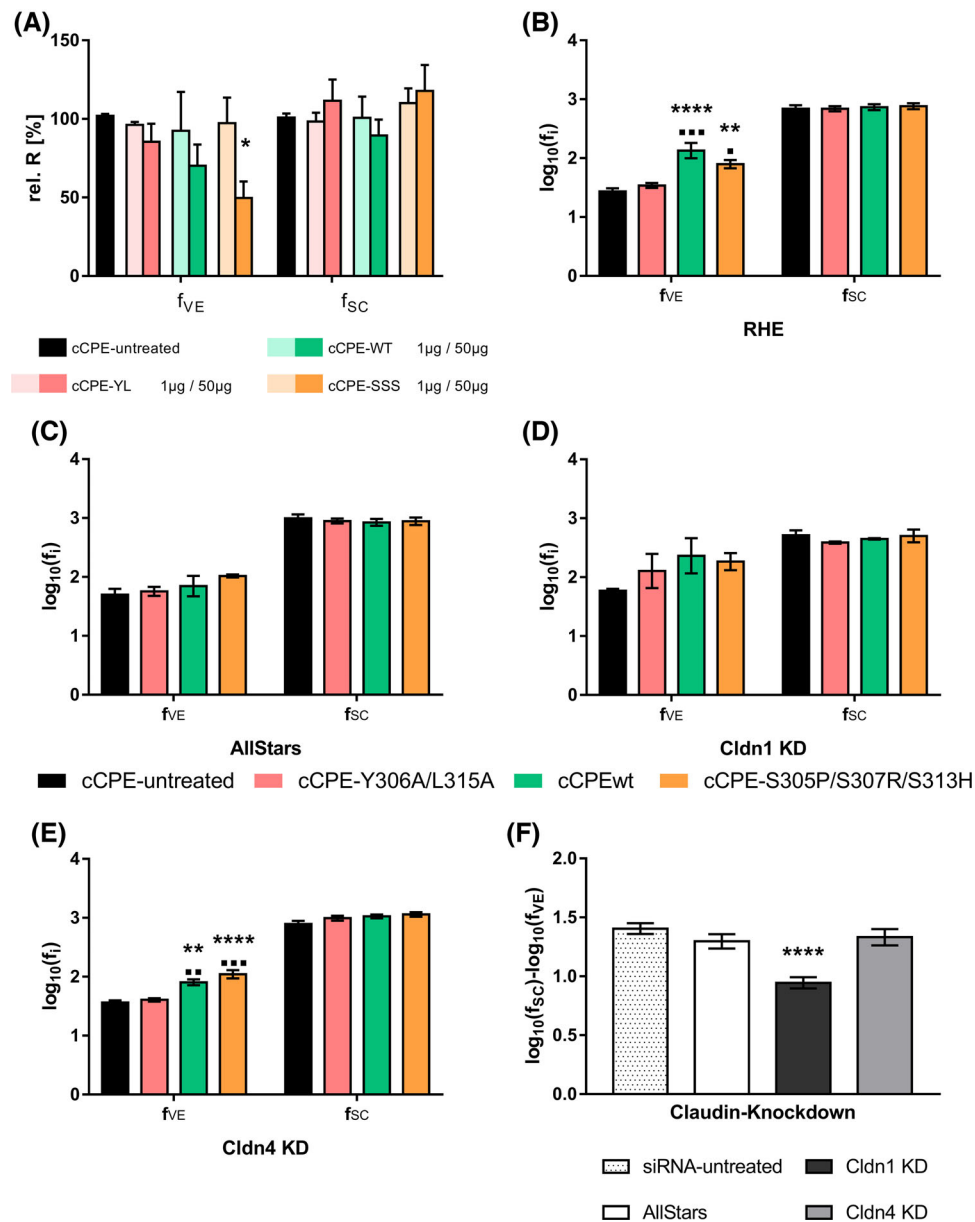
FIGURE 3 *In vitro* modulation of an epidermal barrier by targeting claudin-1 and -4. Impedance spectroscopy measurement in RHE following 24 h incubation with high and low GST-cCPE concentrations from the basal side. (A) Relative resistances of VE and SC derived from peak fitting of relaxation frequencies after 24 h incubation with 1 and 50 µg/ml GST-cCPE. (B–E) Relaxation frequencies after cCPE incubation without siRNA (B) and with siRNA treatment with AllStars control (C), Cldn1 (D), and -4 (E). (F) Differences in relaxation frequencies of SC and VE of cCPE-untreated conditions from siRNA treatments in panels B to E. Mean ± SEM. (A) $n = 3$ for cCPE (1 µg/ml), $n = 6$ for untreated, and $n = 7$ for cCPE (50 µg/ml). (B) $n = 8$, (C–E) $n = 4$. For tests applied, see Methods. * versus control (untreated), ■ versus cCPE-YL. *, ■ $p < 0.05$; **, ■■ $p < 0.01$; ■■■ $p < 0.001$; **** $p < 0.0001$.

binding after the long incubation period (Figure 4I,L). Remarkably, even after the long incubation period with barrier-modulating cCPE, there were still occludin-positive spots at the cell–cell contacts in the SG2 where the signals for GST-cCPEwt and -SSS stopped. At these positions, TJs forming a barrier to larger molecules should still be present (Figure 4J,K, arrows). GST-cCPE incubation also did not induce removal of Cldn1 from the plasma membrane, for example, by endocytosis of claudin–cCPE complexes (Figure 4G–I).

Overall, the morphology of the RHE was not changed due to GST-cCPE incubation. This suggests that the presence of

TJ-modulating agents does not affect the stratification and morphological organization of the epithelium.

Impedance spectroscopy measurements (Figure 3) and immunofluorescence staining (Figures 4 and S2) did not reveal major differences between GST-cCPE variants. This was somewhat surprising, as Cldn1 has been known to have a greater effect on the epidermal barrier than Cldn4,[33] and GST-cCPE-SSS binds with a much higher affinity to Cldn1 than cCPEwt.[24,31,32] Hence, we further investigated the interaction between the GST-cCPE variants and respective claudins in our model systems.
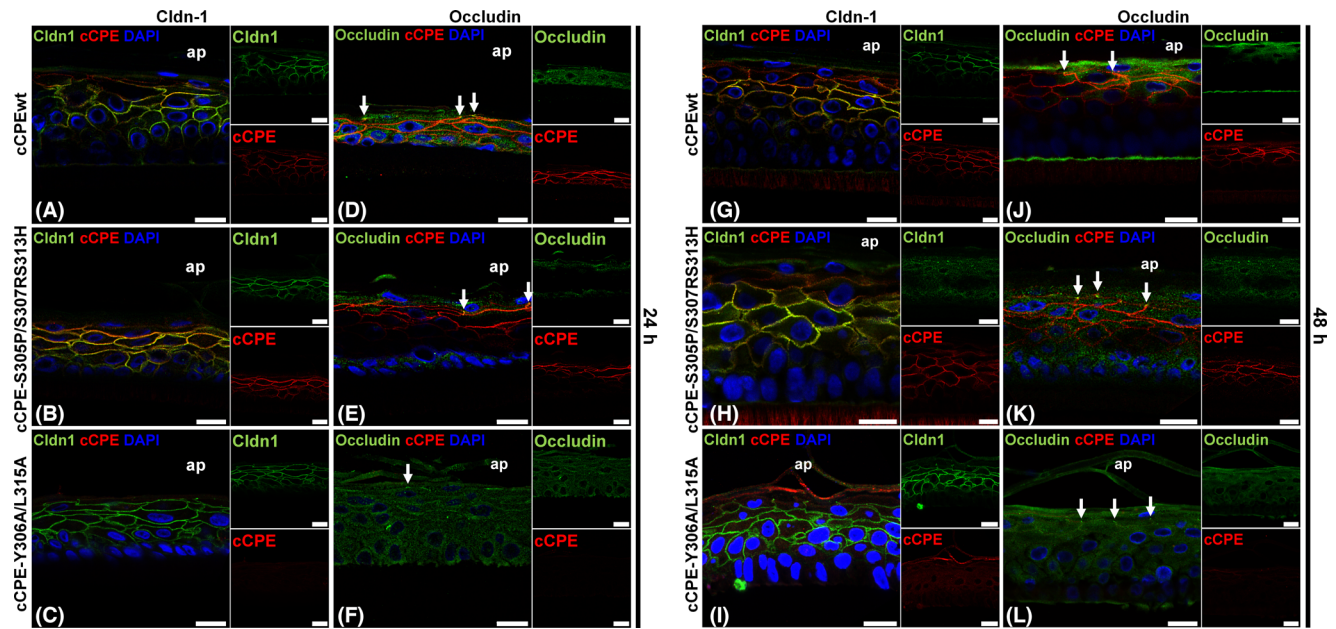
FIGURE 4 GST-cCPE variants bind to extrajunction claudins in reconstructed human epidermis but are stopped at the tight junction. Representative confocal microscopy images of RHE (day 4/5 ALI) paraffin sections after 24 (A–F) and 48 (G–L) h of GST-cCPE incubation (50 μg/ml, basal). (A–C, G–I) Occludin-positive cells (TJs) are marked by an arrow. cCPEwt (A,G) and -SSS (B,H) bind in all layers of RHE. Occludin-positive areas in the apex of the lateral membrane, where GST-cCPE signal stops, could indicate functional TJs. (D–F, J–L) Cldn1 is expressed in all RHE layers, extrajunctional localization in the entire plasma membrane of keratinocytes (not restricted to TJs). Binding of GST-cCPEwt (D,J) and -SSS (E,K) colocalized with Cldn1 signal (yellow in merged image). (C,F,I,L) No specific binding of GST-cCPE-YL at cell–cell contacts. Ap, apical side of RHE (facing ALI). Scale bar = 50 μm.

Colocalization between the GST-cCPE variants and Cldn1 and Cldn4 in RHE after 24 h of incubation was quantified (Figure 5D,E) to estimate the extent of their interaction. Colocalization of both claudins with GST-cCPE-YL was determined to account for unspecific signals (Pearson's coefficient $R \sim 0.4$). GST-cCPEwt and -SSS showed similar colocalization with Cldn1 at low (1 and 10 μg/ml) concentrations, while at 50 μg/ml, GST-cCPE-SSS showed a stronger colocalization than GST-cCPEwt (Figure 5D). Whereas colocalization of GST-cCPEwt and Cldn4 was in the range of the background signal at 1 μg/ml, GST-cCPE-SSS already showed noticeable colocalization. However, at higher concentrations, both GST-cCPEwt and -SSS colocalized with Cldn4 to a similar extent (Figure 5E). This is also reflected in the affinity assays for Cldn4 and GST-cCPEwt or -SSS. At low concentrations, a considerably stronger binding signal was detected for GST-cCPE-SSS compared to -wt. Yet, at higher concentration (>100 nM, 4 μg/ml), the binding of both GST-cCPE variants was in saturation, explaining the same degree of colocalization for both GST-cCPE variants that was detected via colocalization analysis (Figure 5E). Determination of the equilibrium dissociation constant K_D confirmed that GST-cCPE-SSS has a substantially higher affinity for Cldn4 than GST-cCPEwt ($K_D = 9.72 \pm 0.79$ nM for GST-cCPE-SSS and Cldn4; $K_D = 25.62 \pm 2.11$ nM for GST-cCPEwt and Cldn4; Figure 5G) but is still in the same order of magnitude, reflecting the lack of difference in binding behavior in our study.

Nonetheless, the claudin specificity (indicated by the difference to GST-cCPE-YL) and the overall concentration dependency found in the colocalization study confirm that the impaired VE barrier after GST-cCPEwt and -SSS treatment is, indeed, claudin-mediated, that is, due to directed weakening of the TJ barrier.

GST-cCPE variants increase the paracellular permeability for small molecules

In addition to measuring electrical impedance to gauge the permeability for ions, we also used a paracellular molecular tracer assay to assess the TJ permeability for small molecules as an independent method for detection of cCPE-induced barrier opening (Figure 6).

Basally applied NHS-fluorescein (NHS-FL, MW = 473 Da) was able to penetrate all viable layers of the RHE but was prevented from diffusing into the apical membrane of SG2 keratinocytes at intact TJs (Figure 6C, insets show the exclusion of NHS-FL signal from the apical membrane). Co-staining of NHS-FL and ZO1 confirmed that penetration stopped at distinct ZO1-positive structures in SG2, supporting the notion of an intact TJ barrier in VE that seals the paracellular space against small molecules (Figure S2I–L). Quantification of the NHS-FL signal intensity in the basal and apical cell membranes revealed that GST-cCPEwt and SSS but not GST-cCPE-YL led to a concentration-dependent increase in permeability for NHS-FL (Figure 6A–D). Again, the barrier-modulating properties of GST-cCPEwt and -SSS were in a similar range (Figure 6D).

In general, the TJs in native, untreated RHE provided a tight barrier against ions and small and larger molecules. Directed modulation of the TJs by claudin targeting impaired this barrier and increased paracellular diffusion of ions and small molecules. Cldn1 and -4 KD confirmed that Cldn1 is essential for the formation of a functional VE barrier. GST-cCPE treatment indicated that—in addition to Cldn1—Cldn4 may contribute to the maintenance of the VE barrier.
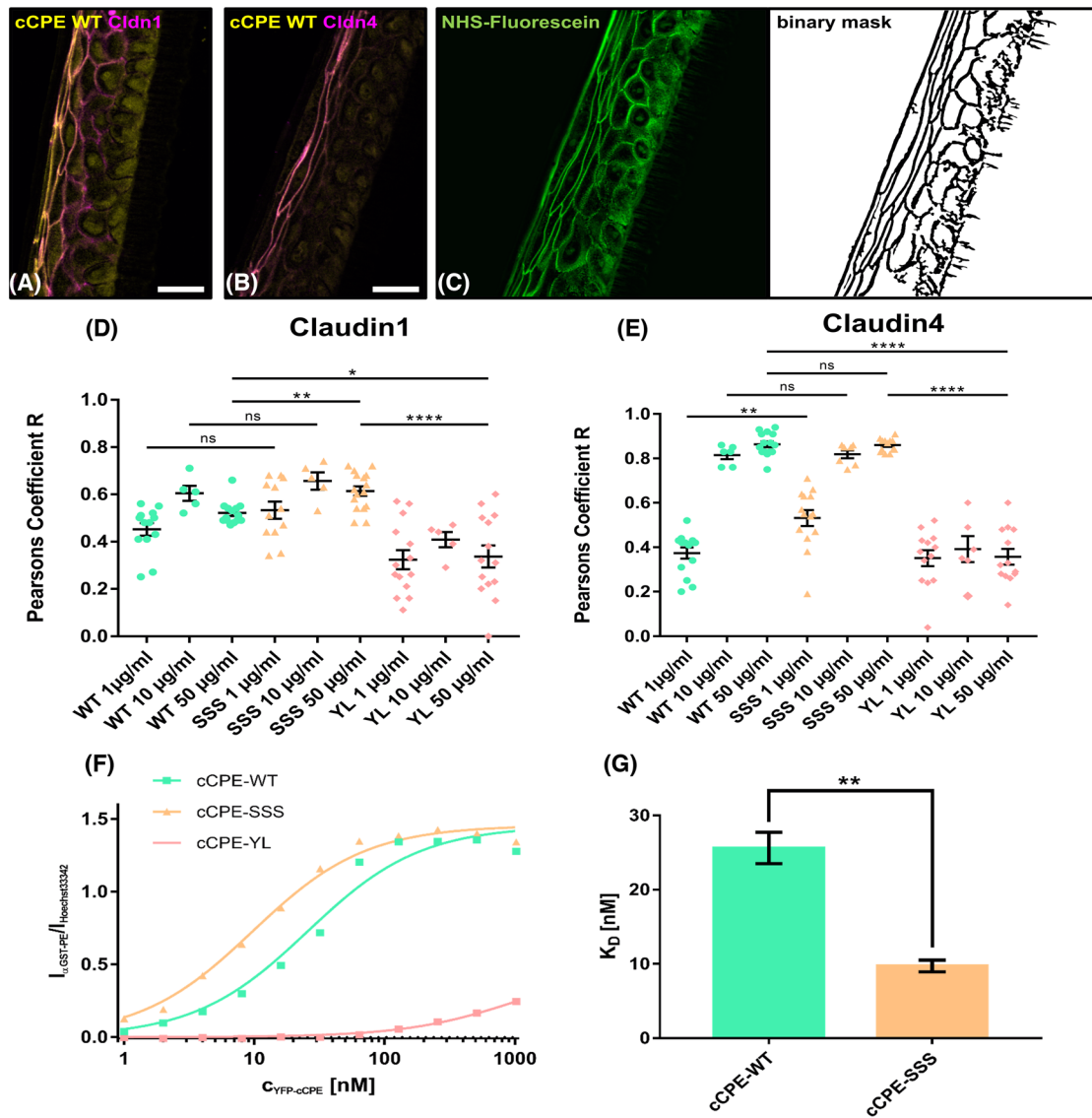
FIGURE 5 GST-cCPE variants colocalize to a similar extent with claudin-1 and -4 at cell–cell contacts in reconstructed human epidermis. (A,B) Representative confocal images of colocalization between GST-cCPEwt and Cldn1 (A) and Cldn4 (B) in the paraffin section of RHE after 24 h of GST-cCPE incubation. (C) An exemplary depiction of a binary mask generated from paracellular NHS-fluorescein used for segmentation in Pearson correlation coefficient determination in panels D and E. (D,E) Colocalization between Cldn1 (D) or Cldn4 (E) and GST-cCPEwt, -SSS, and -YL at 1, 10, and 50 µg/ml. $n = 5–16$, varying between conditions. (F,G) Binding affinity assay for GST-cCPE variants against Cldn4 on transfected Hek293 cells (F) and K_D values for GST-cCPEwt and –SSS derived by nonlinear regression analysis. Mean $\pm$ SEM. $n = 3$. Mann–Whitney test with posthoc Holm–Sidak correction; ns $p > 0.05$; *$p < 0.05$, **$p < 0.01$; ****$p < 0.0001$. Scale bars = 20 µm.

DISCUSSION

The main goal of the present study was to achieve and resolve a controlled modulation of the VE barrier and assess its contribution to the overall epidermal barrier. This was achieved by combining directed targeting of VE barrier components, that is, claudins, by GST-cCPE variants and claudin KD with functional barrier assessment by impedance spectroscopy and tracer molecule permeability.

We could show that intact TJs in the epidermis limit the uncontrolled paracellular flux of ions and small and large molecules (Figures 3, 4, and 6), underscoring the significance of the TJs in addition to the SC in sealing the epidermal barrier. Targeting of Cldn1 and Cldn4 enabled directed modulation of the VE barrier in a claudin- (Figure 3) and dose-dependent manner (Figure 6). Many pathologic skin conditions are also associated with claudin downregulation or loss of function in the epidermis.[7,16,17,19,25] Comprehensive insight into the exact
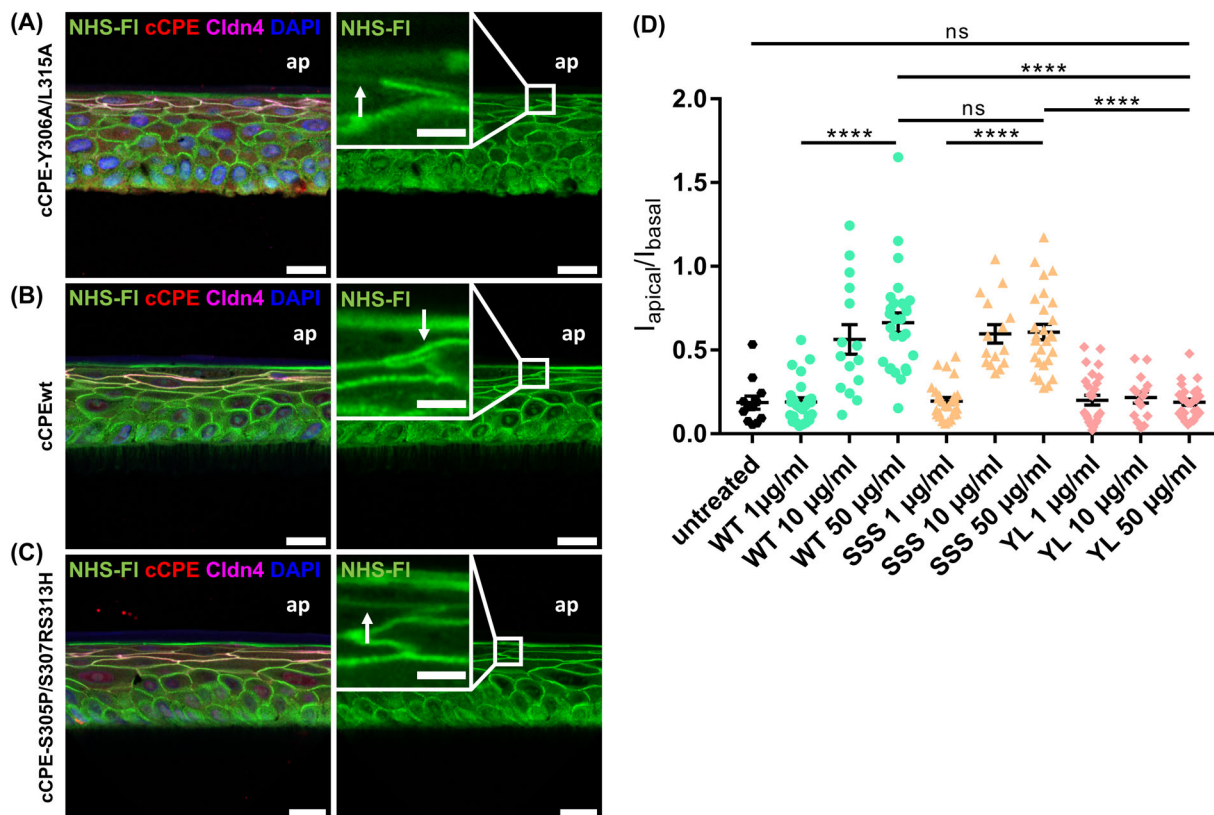
FIGURE 6 Concentration-dependent increase of paracellular permeability for small molecules in reconstructed human epidermis by cCPE variants. Representative confocal images showing exclusion (A) and penetration (B,C) of NHS-FL (0.5 mg/ml, 40 min) into RHE after incubation with GST-cCPE variants (10 μg/ml, 24 h). ap, apical side of RHE; arrow indicates NHS-FL in the apical membrane; scale bar = 20 μm (5 μm in insets). (D) Quantification of NHS-FL permeability by analysis of NHS-FL signal intensity in the apical and basolateral cell membrane of cells in the SG2. $n = 12$ for untreated, $n = 15$ for 10 μg/ml conditions, and $n = 27$ for 1 and 50 μg/ml conditions. Mann–Whitney test with posthoc Holm–Sidak correction. Mean ± SEM. ns $p > 0.05$, ****$p < 0.0001$.

contribution of Cldn1 and -4 to the overall epidermal barrier and the pathogenic consequences of their alterations are still lacking but are required to either restore a functional epidermal barrier in patients or to establish a claudin-directed therapy approach for a deliberate modulation of the epidermal barrier. We were able to confirm the importance of Cldn1 for establishing and maintaining a tight epidermal barrier, and suggest a barrier-regulating role for Cldn4.

Previous studies in mice or human *in vitro* skin models employed claudin KD/knockout, TER measurements, tracer molecule flux, and water loss experiments to show that Cldn1 is essential for the epidermal barrier against ions, water, and larger solutes,[4,7,33] with dose-dependent regulation of the barrier function and associated pathogenicity upon Cldn1 deregulation.[7,45] However, KD of Cldn1 in RHE also resulted in alterations of structural proteins and lipids in the SC.[43] Cldn1 localization was also detected in the lateral cell membranes of the lower layers of SC. These proposed TJ remnants are in close proximity to corneodesmosomes, the main intercellular adhesive structure in the SC that are essential for an orchestrated desquamation process under physiologic skin conditions. TJ remnants are suggested to protect corneodesmosomes against premature degradation during desquamation.[46,47] Hence, Cldn1 KD might not only affect the VE barrier but also lead to dysregulation of SC desquamation that would diminish the SC barrier. Thus, impairment of the epidermal barrier by Cldn1 KD could either be directly ascribed to alterations of the TJs in the VE or indirectly to alterations of SC barrier development.

The function of Cldn4 remains controversial. Experiments using submerged keratinocyte monolayers, which do not represent a stratified epithelium, revealed a role for both Cldn1 and -4 in forming a barrier for ions and small molecules (i.e., sealing pore and leak pathways). However, only Cldn1 was indispensable for a barrier against macromolecules.[35] In contrast, drug-induced downregulation of Cldn4 in human skin led to an increased permeability for a paracellular tracer of ∼ 550 Da[48] and targeting of Cldn4 in normal human keratinocytes grown as a monolayer by a monoclonal anti-Cldn4 antibody attenuated the paracellular barrier.[49] Adding to the controversy, Cldn4 KO mice do not show an obvious skin phenotype,[50] and in RHE, Cldn4 KD did not affect the epidermal barrier.[33]

In addition to long-term inhibition of claudin gene expression by KO or KD experiment, short-term inhibition of claudin proteins by GST-cCPE variants was employed for claudin targeting. This impaired the ion barrier and increased permeability for Lucifer Yellow in RHE.[24]

Here, we combined previous approaches (claudin targeting by siRNA and GST-cCPE, differentiation between the VE and SC barriers by impedance spectroscopy, and permeability tracer imaging)

with the aim to obtain additional information about epidermal barrier components.

Differential contribution of claudin-1 and -4 to the epidermal barrier

Our combined approach enabled us to further dissect the contribution of the individual claudins to the epidermal barrier in more detail.

Our experiments confirmed previous findings that Cldn1 is essential for the formation of a tight epidermal barrier. In addition, we demonstrate that not only a reduction of Cldn1 during stratification but also the subsequent removal of Cldn1 from established TJs is adequate to reduce barrier function (Figures 3 and 6).

In our study, downregulation of Cldn4 during epidermal stratification did not seem to affect the tightness of the VE barrier (Figure 3E,F). Nonetheless, (1) Cldn4 KD led to a weaker GST-cCPEwt (preferential Cldn4-binding) effect on the barrier relative to the GST-cCPE-SSS effect, and (2) the expression of Cldn4 in the epidermis is limited to the SG, where functional TJs are found (Figure 2). This hints at a distinct regulatory role for Cldn4 in the epidermal TJ barrier and may support the notion that not individual TJ proteins but the coordinated functions of multiple TJ components act together to form a tight epidermal seal.

Claudins in the epidermis as therapeutic targets

Claudins have been suggested as targets for numerous therapeutic approaches. These include, among others, treatment of carcinomas,[36,51] visualization of precancerous lesions by means of their associated claudin overexpression,[52–54] or opening of tissue barriers, like the blood–brain barrier[21,22,55] and intestinal barrier[56–58] in a therapeutic context.

In a similar way, transient opening of the epidermal barrier could be beneficial to enhance transdermal drug delivery. This noninvasive route of delivery poses numerous advantages—it avoids first-pass metabolism by digestive enzymes, as is often observed after oral administration, thus improving the bioavailability of the compound and resulting in a constant plasma drug concentration.[20]

Current chemical enhancers used to increase epidermal permeability act by rather unspecific means, for example, by solubilization of lipids and denaturing of keratins, or changing the physicochemical and hydrating properties of the SC.[59,60] A better understanding of the skin barrier components, especially in the VE, is needed for the successful development of directed and effective, but also gentle and reversible, permeability enhancers.

Claudin targeting in the epidermis by GST-cCPE variants to enhance epidermal permeability

In a previous study, we showed that GST-cCPE variants were able to decrease the TER of RHE models.[24] However, using the standard TER measurements, it was not possible to determine whether these effects are limited to claudin inhibition in the VE barrier or might also affect the SC, as was shown for Cldn1 KD in earlier work.[4,33] Direct assessment of the epidermal barrier components by impedance spectroscopy now allowed us to resolve barrier modulation by GST-cCPE variants in more detail and confirmed a claudin-mediated effect, which is limited to the VE barrier (Figure 3).

As formerly reported,[24] both GST-cCPE variants affected ion permeability to a similar degree, even though they possess vastly different affinities for Cldn1. Analysis of colocalization between the GST-cCPE variants and Cldn1 and -4 revealed similar long-term binding behaviors of the GST-cCPE variants to either claudin (Figure 5). At high concentrations (10 and 50 μg/ml) of GST-cCPE, which were able to open the VE barrier (Figures 3, 4, and 6), GST-cCPEwt showed considerable binding to Cldn1 despite the relatively low affinity of GST-cCPEwt for Cldn1. This is likely related to the fact that these concentrations are in the range of, or higher than, the corresponding K_D (~300 nM [12 μg/ml] for binding of GST-cCPEwt to Cldn1[24,61]). However, a low GST-cCPE concentration (1 μg/ml) in the range of the K_D of GST-cCPEwt for Cldn4 (~10–25 nM, 0.4–1 μg/ml; Figure 6G, data not shown, and Ref. 29) and that of GST-cCPE-SSS for Cldn1 and Cldn4 (~10 nM, 0.4 μg/ml; Figure 6G and Ref. 24) did not have a clear effect on ion or small molecule permeability. At a similarly low concentration, GST-cCPEwt specifically removed Cldn4 but not Cldn1 from the TJs of MDCK I cell monolayers.[29] However, in the multilayered RHE, at this concentration, efficient claudin blocking might have been potentially hindered by partial cCPE degradation or limited diffusion toward the TJ-containing SG, to which capture of GST-cCPE by the high amount of extrajunctional Cldn1 in the lower layers of the VE might have contributed. Thus, the use of concentrations in which the different affinities of GST-cCPE-SSS and -wt toward Cldn1 could have been used for efficient differential inhibition of Cldn1 by the two cCPE variants was hampered in the multilayered epidermal tissue. To achieve a more claudin subtype—specific modulation of the TJs, application of cCPE variants with a reduced binding spectrum, in particular, cCPE-S231R/S313H with further increased affinity for Cldn1,[36] and cCPE-L254A/S256A/I258A/D284A[62] with preferential binding to Cldn4, might be beneficial. In addition, subtype-specific anti-claudin antibodies or peptidomimetics could be tested.[63,64] In monolayered normal human keratinocytes, a modified His-cCPE variant with a high affinity for Cldn1, -2, -4, and -5 had similar TJ-modulating effects as a monoclonal anti-Cldn1 antibody.[49] Furthermore, antibody-type claudin binders have a high production cost, making them less attractive for clinical use than small recombinant proteins.

In this study, we could demonstrate a claudin-dependent effect of GST-cCPE variants on the epidermal barrier. We could show that the paracellular pathway for small ions and small molecules (e.g., NHS-FL, 473 Da) but not for macromolecules (≥ ~40 kDa, e.g., GST-cCPE) is affected in a concentration-dependent manner (Figures 3, 4, and 6). This finding of a size-selective modulation is relevant in the context of enhanced transdermal drug delivery since transdermally delivered drugs frequently are small molecules (e.g., diclofenac [296.1 Da[63],
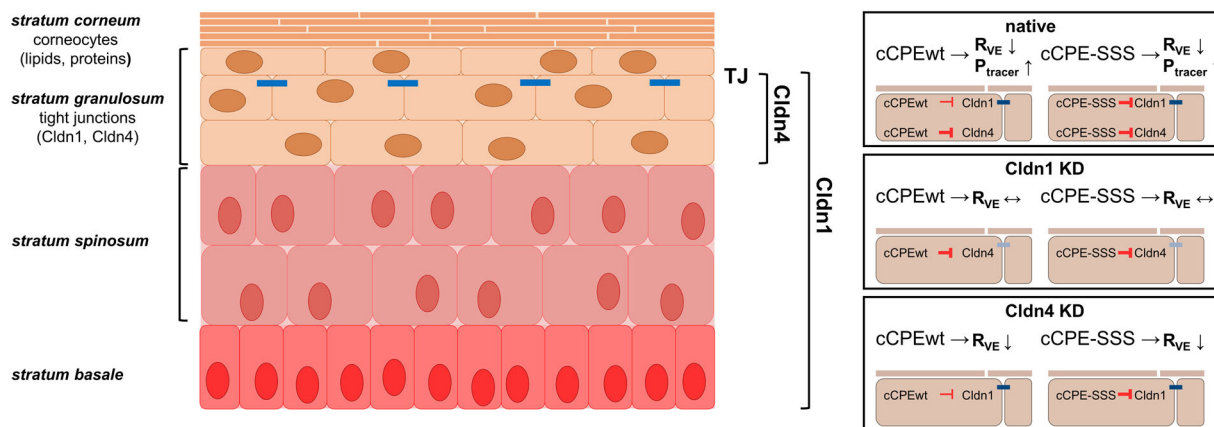
FIGURE 7 Modulation of an epidermal barrier by cCPE variants and claudin KD reveals distinct roles of claudin-1 and -4. TJs (blue bars) in RHE between viable cells of SG2. Cldn1 is expressed in all RHE layers, Cldn4 only in SG. GST-cCPEwt binds Cldn4 with high and Cldn1 with low affinity, whereas GST-cCPE-SSS binds with high affinity to Cldn4 and -1. Native RHE: both GST-cCPEwt and -SSS impair the paracellular barrier against ions (R_{VE}) and smaller molecules (P_{tracer}) in the VE by targeting Cldn1 and Cldn4. Cldn1-KD RHE: leads to loss of tight paracellular barrier (light blue bars) that might mask possible effects due to Cldn4 blocking. Cldn4-KD RHE: does not impede the formation of a tight paracellular barrier. The remaining Cldn1 supports GST-cCPE-SSS impairment of paracellular barrier against ions (R_{VE}) and smaller molecules (P_{tracer}) in the VE. None of the treatments impaired the SC barrier. Whereas Cldn1 appears to be essential for VE barrier formation, Cldn4 might support VE barrier integrity. (See also Figure S1 and the related references.)[67–69]

oxycodone [315.4 Da[44]], or nicotine [162.23 Da[65]]). However, it is of note that here we applied the GST-cCPE variants basally (inside-out) since apical addition of GST-cCPE-containing medium was not compatible with preserving the ALI. Yet, for transdermal drug delivery (outside-in), apical application of cCPE most likely together with additives that affect the SC barrier would be necessary.

Importantly, the epidermal morphology was unchanged after GST-cCPE incubation and functional TJs could still be detected by means of immunofluorescence (Figure 4), indicating a limitation of barrier impairment. This demonstrates the general feasibility of directed TJ-targeting in stratified epithelia and serves as a proof-of-concept for the application of cCPE variants to modulate the epidermal barrier for therapeutic applications. Ideally, enhancers of epidermal permeability would modulate both the SC and VE barrier. Hence, cCPE could be used in combination with current chemical enhancers, such as surface-active agents, fatty acid esters, terpenes, and solvents. To this end, toxicological studies conducted with cCPE variants demonstrated no systemic toxicity and low antigenicity.[66]

In this study, we were able to attribute the barrier-modulating effects of GST-cCPE variants to precise claudin-mediated action and TJ impairment. Our data demonstrate a proof-of-concept for the modulation of the epidermal barrier by targeting Cldn1 and -4, and confirm a differential contribution of either claudin to the skin barrier (Figure 7). Whereas Cldn1 is required for the formation of a tight epidermal barrier, Cldn4—if at all—might only support barrier integrity.

AUTHOR CONTRIBUTIONS
L.-S.B, R.M., J.P., and D.G. conceived the study. S.V.-Y.-S. generated R.H.E. models and L.-S.B., A.W., S.K.F., and R.M. performed experiments. A.W. implemented image analysis. L.-S.B., A.W., S.K.F., R.M., J.P., and D.G. analyzed experimental data. L.-S.B. wrote the manuscript with contributions and edits from A.W., S.K.F., J.M.B., J.P., and D.G. All authors approved the final version of the manuscript.

COMPETING INTERESTS
The authors declare no competing interests.

PEER REVIEW
The peer review history for this article is available at: https://publons.com/publon/10.1111/nyas.14879.

ORCID
Jörg Piontek https://orcid.org/0000-0002-0880-8915
Dorothee Günzel https://orcid.org/0000-0002-7998-7164

REFERENCES
1. Proksch, E., Brandner, J. M., & Jensen, J.-M. (2008). The skin: An indispensable barrier. *Experimental Dermatology*, 17, 1063–1072.
2. Lee, A.-Y. (2020). Molecular mechanism of epidermal barrier dysfunction as primary abnormalities. *International Journal of Molecular Sciences*, 21, 1194.
3. Schmitz, A., Lazi'ć, E., Koumaki, D., Kuonen, F., Verykiou, S., & Rübsam, M. (2015). Assessing the in vivo epidermal barrier in mice: Dye penetration assays. *Journal of Investigative Dermatology*, 135, 1–4.
4. Furuse, M., Hata, M., Furuse, K., Yoshida, Y., Haratake, A., Sugitani, Y., Noda, T., Kubo, A., & Tsukita, S. (2002). Claudin-based tight junctions are crucial for the mammalian epidermal barrier: A lesson from claudin-1-deficient mice. *Journal of Cell Biology*, 156, 1099–1111.
5. Tunggal, J. A., Helfrich, I., Schmitz, A., Schwarz, H., Günzel, D., Fromm, M., Kemler, R., Krieg, T., & Niessen, C. M. (2005). E-cadherin is

essential for in vivo epidermal barrier function by regulating tight junctions. *Embo Journal*, 24, 1146–1156.

6. Günzel, D., & Yu, A. S. L. (2013). Claudins and the modulation of tight junction permeability. *Physiological Reviews*, 93, 525–569.

7. Bergmann, S., Von Buenau, B., Vidal-Y-Sy, S., Haftek, M., Wladykowski, E., Houdek, P., Lezius, S., Duplan, H., Bäsler, K., Dähnhardt-Pfeiffer, S., Gorzelanny, C., Schneider, S. W., Rodriguez, E., Stölzl, D., Weidinger, S., & Brandner, J. M. (2020). Claudin-1 decrease impacts epidermal barrier function in atopic dermatitis lesions dose-dependently. *Science Reports*, 10, 2024.

8. Brandner, J., Zorn-Kruppa, M., Yoshida, T., Moll, I., Beck, L. A., & De Benedetto, A. (2015). Epidermal tight junctions in health and disease. *Tissue Barriers*, 3, e974451.

9. Hou, J., Renigunta, A., Yang, J., & Waldegger, S. (2010). Claudin-4 forms paracellular chloride channel in the kidney and requires claudin-8 for tight junction localization. *Proceedings of the National Academy of Sciences of the United States of America*, 107, 18010–18015.

10. Van Itallie, C., Rahner, C., & Anderson, J. M. (2001). Regulated expression of claudin-4 decreases paracellular conductance through a selective decrease in sodium permeability. *Journal of Clinical Investigation*, 107, 1319–1327.

11. Kezic, S. (2014). Skin barrier in atopic dermatitis. *Frontiers in Bioscience*, 19, 542–556.

12. Koppes, S. A., Engebretsen, K. A., Agner, T., Angelova-Fischer, I., Berents, T., Brandner, J., Brans, R., Clausen, M.-L., Hummler, E., Jakasa, I., Jurakić-Tončic, R., John, S. M., Khnykin, D., Molin, S., Holm, J. O., Suomela, S., Thierse, H.-J., Kezic, S., Martin, S. F., & Thyssen, J. P. (2017). Current knowledge on biomarkers for contact sensitization and allergic contact dermatitis. *Contact Dermatitis*, 77, 1–16.

13. Palmer, C. N. A., Irvine, A. D., Terron-Kwiatkowski, A., Zhao, Y., Liao, H., Lee, S. P., Goudie, D. R., Sandilands, A., Campbell, L. E., Smith, F. J. D., O'regan, G. I. M., Watson, R. M., Cecil, J. O. E., Bale, S. J., Compton, J. G., Digiovanna, J. J., Fleckman, P., Lewis-Jones, S., Arseculeratne, G., … Mclean, W. H. I. (2006). Common loss-of-function variants of the epidermal barrier protein filaggrin are a major predisposing factor for atopic dermatitis. *Nature Genetics*, 38, 441–446.

14. Smith, F. J. D., Irvine, A. D., Terron-Kwiatkowski, A., Sandilands, A., Campbell, L. E., Zhao, Y., Liao, H., Evans, A. T., Goudie, D. R., Lewis-Jones, S., Arseculeratne, G., Munro, C. S., Sergeant, A., O'regan, G. I., Bale, S. J., Compton, J. G., Digiovanna, J. J., Presland, R. B., Fleckman, P., & Mclean, W. H. I. (2006). Loss-of-function mutations in the gene encoding filaggrin cause ichthyosis vulgaris. *Nature Genetics*, 38, 337–342.

15. Schmuth, M., Blunder, S., Dubrac, S., Gruber, R., & Moosbrugger-Martinz, V. (2015). Epidermal barrier in hereditary ichthyoses, atopic dermatitis, and psoriasis. *Journal der Deutschen Dermatologischen Gesellschaft*, 13, 1119–1123.

16. Yokouchi, M., & Kubo, A. (2018). Maintenance of tight junction barrier integrity in cell turnover and skin diseases. *Experimental Dermatology*, 27, 876–883.

17. Sugawara, T., Iwamoto, N., Akashi, M., Kojima, T., Hisatsune, J., Sugai, M., & Furuse, M. (2013). Tight junction dysfunction in the stratum granulosum leads to aberrant stratum corneum barrier function in claudin-1-deficient mice. *Journal of Dermatological Science*, 70, 12–18.

18. Abdel-Gadir, A., Stephen-Victor, E., Gerber, G. K., Noval Rivas, M., Wang, S., Harb, H., Wang, L., Li, N., Crestani, E., Spielman, S., Secor, W., Biehl, H., Dibenedetto, N., Dong, X., Umetsu, D. T., Bry, L., Rachid, R., & Chatila, T. A. (2019). Microbiota therapy acts via a regulatory T cell MyD88/RORgammat pathway to suppress food allergy. *Nature Medicine*, 25, 1164–1174.

19. Hadj-Rabia, S., Baala, L., Vabres, P., Hamel-Teillac, D., Jacquemin, E., Fabre, M., Lyonnet, S., De Prost, Y., Munnich, A., Hadchouel, M., & Smahi, A. (2004). Claudin-1 gene mutations in neonatal sclerosing cholangitis associated with ichthyosis: A tight junction disease. *Gastroenterology*, 127, 1386–1390.

20. Iqbal, B., Ali, J., & Baboota, S. (2018). Recent advances and development in epidermal and dermal drug deposition enhancement technology. *International Journal of Dermatology*, 57, 646–660.

21. Neuhaus, W., Piontek, A., Protze, J., Eichner, M., Mahringer, A., Subileau, E.-A., Lee, I. N.-F. M., Schulzke, J. D., Krause, G., & Piontek, J. (2018). Reversible opening of the blood–brain barrier by claudin-5-binding variants of *Clostridium perfringens* enterotoxin's claudin-binding domain. *Biomaterials*, 161, 129–143.

22. Breitkreuz-Korff, O., Tscheik, C., Del Vecchio, G., Dithmer, S., Walther, W., Orthmann, A., Wolburg, H., Haseloff, R. F., Schröder, L., Blasig, I. E., & Winkler, L. (2021). M01 as a novel drug enhancer for specifically targeting the blood–brain barrier. *Journal of Controlled Release*, 338, 137–148.

23. Alexander, H., Brown, S., Danby, S., & Flohr, C. (2018). Research techniques made simple: Transepidermal water loss measurement as a research tool. *Journal of Investigative Dermatology*, 138, 2295–2300. e1.

24. Beier, L.-S., Rossa, J., Woodhouse, S., Bergmann, S., Kramer, H., Protze, J., Eichner, M., Piontek, A., Vidal-Y-Sy, S., Brandner, J., Krause, G., Zitzmann, N., & Piontek, J. (2019). Use of modified *Clostridium perfringens* enterotoxin fragments for claudin targeting in liver and skin cells. *International Journal of Molecular Sciences*, 20, 4774.

25. De Benedetto, A., Rafaels, N. M., Mcgirt, L. Y., Ivanov, A. I., Georas, S. N., Cheadle, C., Berger, A. E., Zhang, K., Vidyasagar, S., Yoshida, T., Boguniewicz, M., Hata, T., Schneider, L. C., Hanifin, J. M., Gallo, R. L., Novak, N., Weidinger, S., Beaty, T. H., Leung, D. Y. M., … Beck, L. A. (2011). Tight junction defects in patients with atopic dermatitis. *Journal of Allergy and Clinical Immunology*, 127, 773–786.e7.e1–7.

26. Shan, J., Oshima, T., Chen, X., Fukui, H., Watari, J., & Miwa, H. (2012). Trypsin impaired epithelial barrier function and induced IL-8 secretion through basolateral PAR-2: A lesson from a stratified squamous epithelial model. *American Journal of Physiology-Gastrointestinal and Liver Physiology*, 303, G1105–G1112.

27. Pradal, J., Vallet, C., Frappin, G., Bariguian, F., & Lombardi, M. S. (2019). Importance of the formulation in the skin delivery of topical diclofenac: Not all topical diclofenac formulations are the same. *Journal of Pain Research*, 12, 1149–1154.

28. Shrestha, A., Uzal, F. A., & Mcclane, B. A. (2016). The interaction of *Clostridium perfringens* enterotoxin with receptor claudins. *Anaerobe*, 41, 18–26.

29. Sonoda, N., Furuse, M., Sasaki, H., Yonemura, S., Katahira, J., Horiguchi, Y., & Tsukita, S. (1999). *Clostridium perfringens* enterotoxin fragment removes specific claudins from tight junction strands: Evidence for direct involvement of claudins in tight junction barrier. *Journal of Cell Biology*, 147, 195–204.

30. Winkler, L., Gehring, C., Wenzel, A., Müller, S. L., Piehl, C., Krause, G., Blasig, I. E., & Piontek, J. (2009). Molecular determinants of the interaction between *Clostridium perfringens* enterotoxin fragments and claudin-3. *Journal of Biological Chemistry*, 284, 18863–18872.

31. Takahashi, A., Saito, Y., Kondoh, M., Matsushita, K., Krug, S. M., Suzuki, H., Tsujino, H., Li, X., Aoyama, H., Matsuhisa, K., Uno, T., Fromm, M., Hamakubo, T., & Yagi, K. (2012). Creation and biochemical analysis of a broad-specific claudin binder. *Biomaterials*, 33, 3464–3474.

32. Protze, J., Eichner, M., Piontek, A., Dinter, S., Rossa, J., Blecharz, K. G., Vajkoczy, P., Piontek, J., & Krause, G. (2015). Directed structural modification of *Clostridium perfringens* enterotoxin to enhance binding to claudin-5. *Cellular and Molecular Life Sciences*, 72, 1417–1432.

33. Mannweiler, R., Bergmann, S., Vidal-Y-Sy, S., Brandner, J. M., & Günzel, D. (2021). Direct assessment of individual skin barrier components by electrical impedance spectroscopy. *Allergy*, 76, 3094–3106.

34. Bäsler, K., Galliano, M.-F., Bergmann, S., Rohde, H., Wladykowski, E., Vidal-Y-Sy, S., Guiraud, B., Houdek, P., Schüring, G., Volksdorf, T., Caruana, A., Bessou-Touya, S., Schneider, S. W., Duplan, H., & Brandner, J. M. (2017). Biphasic influence of *Staphylococcus aureus* on human epidermal tight junctions. *Annals of the New York Academy of Sciences*, 1405, 53–70.

35. Kirschner, N., Rosenthal, R., Furuse, M., Moll, I., Fromm, M., & Brandner, J. M. (2013). Contribution of tight junction proteins to ion, macromolecule, and water barrier in keratinocytes. *Journal of Investigative Dermatology*, *133*, 1161–1169.

36. Piontek, A., Eichner, M., Zwanziger, D., Beier, L. S., Protze, J., Walther, W., Theurer, S., Schmid, K. W., Führer-Sakel, D., Piontek, J., & Krause, G. (2020). Targeting claudin-overexpressing thyroid and lung cancer by modified *Clostridium perfringens* enterotoxin. *Molecular Oncology*, *14*, 261–276.

37. Castro Dias, M., Odriozola Quesada, A., Soldati, S., Bösch, F., Gruber, I., Hildbrand, T., Sönmez, D., Khire, T., Witz, G., Mcgrath, J. L., Piontek, J., Kondoh, M., Deutsch, U., Zuber, B., & Engelhardt, B. (2021). Brain endothelial tricellular junctions as novel sites for T cell diapedesis across the blood–brain barrier. *Journal of Cell Science*, *134*, jcs253880.

38. Piontek, A., Witte, C., May Rose, H., Eichner, M., Protze, J., Krause, G., Piontek, J., & Schröder, L. A. (2017). cCPE-based xenon biosensor for magnetic resonance imaging of claudin-expressing cells. *Annals of the New York Academy of Sciences*, *1397*, 195–208.

39. Fujita, K., Katahira, J., Horiguchi, Y., Sonoda, N., Furuse, M., & Tsukita, S. (2000). *Clostridium perfringens* enterotoxin binds to the second extracellular loop of claudin-3, a tight junction integral membrane protein. *FEBS Letters*, *476*, 258–261.

40. Kimura, J., Abe, H., Kamitani, S., Toshima, H., Fukui, A., Miyake, M., Kamata, Y., Sugita-Konishi, Y., Yamamoto, S., & Horiguchi, Y. (2009). *Clostridium perfringens* enterotoxin interacts with claudins via electrostatic attraction. *Journal of Biological Chemistry*, *285*, 401–408.

41. Shrestha, A., & Mcclane, B. A. (2013). Human claudin-8 and -14 are receptors capable of conveying the cytotoxic effects of *Clostridium perfringens* enterotoxin. *mBio*, *4*, e00594–12.

42. Brandner, J. M., Kief, S., Wladykowski, E., Houdek, P., & Moll, I. (2006). Tight junction proteins in the skin. *Skin Pharmacology and Physiology*, *19*, 71–77.

43. Yoshida, K., Yokouchi, M., Nagao, K., Ishii, K., Amagai, M., & Kubo, A. (2013). Functional tight junction barrier localizes in the second layer of the stratum granulosum of human epidermis. *Journal of Dermatological Science*, *71*, 89–99.

44. Eichner, M., Augustin, C., Fromm, A., Piontek, A., Walther, W., Bücker, R., Fromm, M., Krause, G., Schulzke, J., Günzel, D., & Piontek, J. (2017). In colon epithelia, *Clostridium perfringens* enterotoxin causes focal leaks by targeting claudins which are apically accessible due to tight junction derangement. *Journal of Infectious Diseases*, *217*, 147–157.

45. Tokumasu, R., Yamaga, K., Yamazaki, Y., Murota, H., Suzuki, K., Tamura, A., Bando, K., Furuta, Y., Katayama, I., & Tsukita, S. (2016). Dose-dependent role of claudin-1 in vivo in orchestrating features of atopic dermatitis. *Proceedings of the National Academy of Sciences of the United States of America*, *113*, E4061–E4068.

46. Haftek, M., Callejon, S., Sandjeu, Y., Padois, K., Falson, F., Pirot, F., Portes, P., Demarne, F., & Jannin, V. (2011). Compartmentalization of the human stratum corneum by persistent tight junction-like structures. *Experimental Dermatology*, *20*, 617–621.

47. Igawa, S., Kishibe, M., Murakami, M., Honma, M., Takahashi, H., Iizuka, H., & Ishida-Yamamoto, A. (2011). Tight junctions in the stratum corneum explain spatial differences in corneodesmosome degradation. *Experimental Dermatology*, *20*, 53–57.

48. Yuki, T., Hachiya, A., Kusaka, A., Sriwiriyanont, P., Visscher, M. O., Morita, K., Muto, M., Miyachi, Y., Sugiyama, Y., & Inoue, S. (2011). Characterization of tight junctions and their disruption by UVB in human epidermis and cultured keratinocytes. *Journal of Investigative Dermatology*, *131*, 744–752.

49. Nakajima, M., Nagase, S., Iida, M., Takeda, S., Yamashita, M., Watari, A., Shirasago, Y., Fukasawa, M., Takeda, H., Sawasaki, T., Yagi, K., & Kondoh, M. (2015). Claudin-1 binder enhances epidermal permeability in a human keratinocyte model. *Journal of Pharmacology and Experimental Therapeutics*, *354*, 440–447.

50. Kage, H., Flodby, P., Gao, D., Kim, Y. H. o, Marconett, C. N., Demaio, L., Kim, K.-J., Crandall, E. D., & Borok, Z. (2014). Claudin 4 knockout mice: Normal physiological phenotype with increased susceptibility to lung injury. *American Journal of Physiology-Lung Cellular and Molecular Physiology*, *307*, L524–L536.

51. Pahle, J., Kobelt, D., Aumann, J., Behrens, D., Daberkow, O., Mokritzkij, M., Piontek, J., Stein, U., & Walther, W. (2021). Effective oncoleaking treatment of pancreatic cancer by claudin-targeted suicide gene therapy with *Clostridium perfringens* enterotoxin (CPE). *Cancers (Basel)*, *13*, 4393.

52. Neesse, A., Hahnenkamp, A., Griesmann, H., Buchholz, M., Hahn, S. A., Maghnouj, A., Fendrich, V., Ring, J., Sipos, B., Tuveson, D. A., Bremer, C., Gress, T. M., & Michl, P. (2013). Claudin-4-targeted optical imaging detects pancreatic cancer and its precursor lesions. *Gut*, *62*, 1034–1043.

53. Rabinsky, E. F., Joshi, B. P., Pant, A., Zhou, J., Duan, X., Smith, A., Kuick, R., Fan, S., Nusrat, A., Owens, S. R., Appelman, H. D., & Wang, T. D. (2016). Overexpressed claudin-1 can be visualized endoscopically in colonic adenomas in vivo. *Cellular and Molecular Gastroenterology and Hepatology*, *2*, 222–237.

54. Torres, J. B. A., Knight, J. C., Mosley, M. J., Kersemans, V., Koustoulidou, S., Allen, D., Kinchesh, P., Smart, S., & Cornelissen, B. (2018). Imaging of claudin-4 in pancreatic ductal adenocarcinoma using a radiolabelled anti-claudin-4 monoclonal antibody. *Molecular Imaging and Biology*, *20*, 292–299.

55. Winkler, L., Blasig, R., Breitkreuz-Korff, O., Berndt, P., Dithmer, S., Helms, H. C., Puchkov, D., Devraj, K., Kaya, M., Qin, Z., Liebner, S., Wolburg, H., Andjelkovic, A. V., Rex, A., Blasig, I. E., & Haseloff, R. F. (2021). Tight junctions in the blood–brain barrier promote edema formation and infarct size in stroke — Ambivalent effects of sealing proteins. *Journal of Cerebral Blood Flow and Metabolism*, *41*, 132–145.

56. Krug, S. M., Amasheh, M., Dittmann, I., Christoffel, I., Fromm, M., & Amasheh, S. (2013). Sodium caprate as an enhancer of macromolecule permeation across tricellular tight junctions of intestinal cells. *Biomaterials*, *34*, 275–282.

57. Dittmann, I., Amasheh, M., Krug, S. M., Markov, A. G., Fromm, M., & Amasheh, S. (2014). Laurate permeabilizes the paracellular pathway for small molecules in the intestinal epithelial cell model HT-29/B6 via opening the tight junctions by reversible relocation of claudin-5. [Corrected]. *Pharmaceutical Research*, *31*, 2539–2548.

58. Radloff, J., Cornelius, V., Markov, A. G., & Amasheh, S. (2019). Caprate modulates intestinal barrier function in porcine Peyer's patch follicle-associated epithelium. *International Journal of Molecular Sciences*, *20*, 1418.

59. Marwah, H., Garg, T., Goyal, A. K., & Rath, G. (2016). Permeation enhancer strategies in transdermal drug delivery. *Drug Delivery*, *23*, 564–578.

60. Kováčik, A., Kopečná, M., & Vávrová, K. (2020). Permeation enhancers in transdermal drug delivery: Benefits and limitations. *Expert Opinion on Drug Delivery*, *17*, 145–155.

61. Kimura, J., Abe, H., Kamitani, S., Toshima, H., Fukui, A., Miyake, M., Kamata, Y., Sugita-Konishi, Y., Yamamoto, S., & Horiguchi, Y. (2010). *Clostridium perfringens* enterotoxin interacts with claudins via electrostatic attraction. *Journal of Biological Chemistry*, *285*, 401–408.

62. Veshnyakova, A., Piontek, J., Protze, J., Waziri, N., Heise, I., & Krause, G. (2012). Mechanism of *Clostridium perfringens* enterotoxin interaction with claudin-3/-4 protein suggests structural modifications of the toxin to target specific claudins. *The Journal of Biological Chemistry*, *287*, 1698–1708.

63. Dithmer, S., Staat, C., Müller, C., Ku, M.-C., Pohlmann, A., Niendorf, T., Gehne, N., Fallier-Becker, P., Kittel, Ä., Walter, F. R., Veszelka, S., Deli, M. A., Blasig, R., Haseloff, R. F., Blasig, I. E., & Winkler, L. (2017). Claudin peptidomimetics modulate tissue barriers for enhanced drug

delivery. *Annals of the New York Academy of Sciences*, 1397, 169–184.

64. Hashimoto, Y., Okada, Y., Shirakura, K., Tachibana, K., Sawada, M., Yagi, K., Doi, T., & Kondoh, M. (2019). Anti-claudin antibodies as a concept for development of claudin-directed drugs. *Journal of Pharmacology and Experimental Therapeutics*, 368, 179–186.

65. Fanning, A. S., Jameson, B. J., Jesaitis, L. A., & Anderson, J. M. (1998). The tight junction protein ZO-1 establishes a link between the transmembrane protein occludin and the actin cytoskeleton. *Journal of Biological Chemistry*, 273, 29745–29753.

66. Suzuki, H., Kondoh, M., Li, X., Takahashi, A., Matsuhisa, K., Matsushita, K., Kakamu, Y., Yamane, S., Kodaka, M., Isoda, K., & Yagi, K. (2011). A toxicological evaluation of a claudin modulator, the C-terminal fragment of *Clostridium perfringens* enterotoxin, in mice. *Die Pharmazie*, 66, 543–546.

67. Shinoda, T., Shinya, N., Ito, K., Ohsawa, N., Terada, T., Hirata, K., Kawano, Y., Yamamoto, M., Kimura-Someya, T., Yokoyama, S., & Shirouzu, M. (2016). Structural basis for disruption of claudin assembly in tight junctions by an enterotoxin. *Scientific Reports*, 6, 33632.

68. Saitoh, Y., Suzuki, H., Tani, K., Nishikawa, K., Irie, K., Ogura, Y., Tamura, A., Tsukita, S., & Fujiyoshi, Y. (2015). Tight junctions. Structural insight into tight junction disassembly by *Clostridium perfringens* enterotoxin. *Science (New York, N.Y.)*, 347, 775–778.

69. Hempel, C., Protze, J., Altun, E., Riebe, B., Piontek, A., Fromm, A., Lee, I. M., Saleh, T., Günzel, D., Krause, G., & Piontek, J. (2020). Assembly of tight junction strands: Claudin-10b and claudin-3 form homo-tetrameric building blocks that polymerise in a channel-independent manner. *Journal of Molecular Biology*, 432, 2405–2427.

SUPPORTING INFORMATION

Additional supporting information can be found online in the Supporting Information section at the end of this article.